iScience

CellPress
OPEN ACCESS

Article

Construction of hydroxyl-functionalized hyper-crosslinked networks from polyimide for highly efficient iodine adsorption

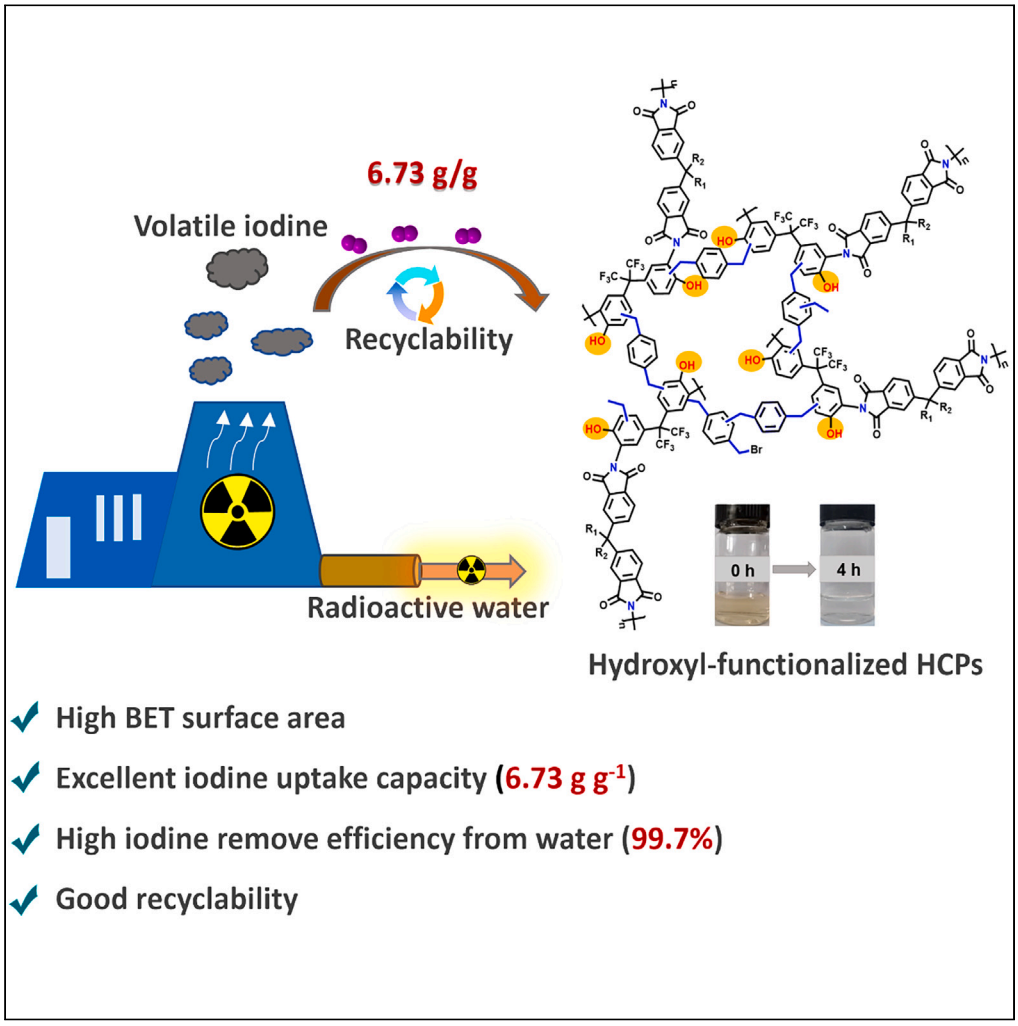

Jianjun Wang, Tingting Wu, Xianlong Wang, ..., Jiao Liu, Liang Xu, Yu Zang

02900@qqhru.edu.cn

Highlights

Two novel hyper-crosslinked polymers were prepared via Friedel-Crafts reaction

The polymers showed a porous morphology, high BET surface areas and good stability

The material exhibits excellent iodine capture performance (6.73 g/g)

They can maintain more than 91% of the absorption capacity after four cycles

Wang et al., iScience 27, 108993
February 16, 2024
https://doi.org/10.1016/j.isci.2024.108993

iScience

CellPress
OPEN ACCESS

Article

Construction of hydroxyl-functionalized hyper-crosslinked networks from polyimide for highly efficient iodine adsorption

Jianjun Wang,[1,2,4,*] Tingting Wu,[1] Xianlong Wang,[1] Jiaqi Chen,[2] Minyi Fan,[2] Zhichun Shi,[2] Jiao Liu,[1] Liang Xu,[3] and Yu Zang[1]

SUMMARY

The rapid development of nuclear energy posed a great threat to the environment and human health. Herein, two hydroxyl-functionalized hyper-crosslinked polymers (PIHCP-1 and PIHCP-2) containing different electron active sites have been synthesized via Friedel-Crafts alkylation reaction of the polyimides. The resulting polymers showed a micro/mesoporous morphology and good thermal and chemical stability. Rely on the high porosity and multi-active sites, the PIHCPs show an ultrahigh iodine uptake capacity reached 6.73 g g^{-1} and the iodine removal efficiency from aqueous solution also reaches 99.7%. Kinetic analysis demonstrates that the iodine adsorption on PIHCPs was happened on the heterogeneous surfaces in the form of multilayer chemisorption. Electrostatic potential (ESP) calculation proves the great contribution of hydroxyl groups on the iodine capture performance. In addition, the iodine capture efficiency of both adsorbents can be maintained over 91% after four cyclic experiments which ensures their good recyclability for further practical applications.

INTRODUCTION

The rapid development of industrialization has leaded to significant emissions of greenhouse gases which cause a huge threat to our environment. Under this circumstance, nuclear power is widely used in global due to its outstanding advantages, such as high efficiency, low CO_2 emission and low-cost.[1,2] However, nuclear leakage and medical waste generate serious radioactive iodine pollutants (^{131}I and ^{129}I) which can severely damage the environment and human metabolic process.[3,4] In particular, the half-life of ^{129}I can reach up to 1.57×10^7 years with high toxic, which not only exist as volatile particles in the air but will also enter the groundwater via rainfall, in further affect human health and even cause cancer.[5] Therefore, dealing with radioactive iodine in water and air is still in a nascent stage. In this regard, researchers are trying to exploit alternative materials for dealing with the radioiodine pollution in water as well as in vapor phase.[6,7]

Recently, functional porous absorbents such as silver-based zeolites[8–10] and metal-organic frameworks (MOFs)[11–13] have been designed for I_2 capture, but their low capture capacity, irreversible procedure and high cost have restricted their development and application. Therefore, multiple porous organic polymers (POPs) have been developed and utilized in adsorption, catalysis, and other fields to solve environmental problems.[14–18] In particular, incorporation of the heterotopic atom has showed a great contribution on enhancing the activity of the porous materials.[19] For example, Mondal et al. explored a Cu-embedded carbazole-derived porous organic polymer (Cu@Cz-POP) nanohybrid for CO_2 electrocarboxylation and demonstrating the importance of heterotopic atom on the electrocatalytic activity.[20] Beyond that, POPs are also extensively utilized on iodine adsorption.[21–24] Very recently, Yan and co-authors constructed a nitrogen-rich semi-cycloaliphatic polyaminal networks (sPANs) via a one-pot method, and the iodine capture capacity was calculated to be 2656 mg g^{-1}.[25] Li et al. synthesized a Carbazole-based porous organic polymer for iodine capture, the obtained polymer showed a high uptake capacity for iodine vapor as 2.86 g g^{-1}.[26] Recently, two bitetrazole-based porous organic polymers have been designed and prepared by Geng's group through nucleophilic substitution reactions, the strong interaction of cyclophosphonitrile unit with iodine contributed an excellent iodine capture performance (5.66 g g^{-1}).[27] Han's group developed ionic covalent organic frameworks (iCOFs) which with ionic active sites to afford high iodine capture capacity up to 10.21 g g^{-1}.[28] All of the results above indicate that the iodine capture capacity of absorbent closely related to their porous morphology as well as the preferential recognition sites on the structure.[29,30]

[1]College of Materials Science and Engineering, Qiqihar University, Wenhua Street 42, Qiqihar, Heilongjiang 161006, China
[2]College of Chemistry and Chemical Engineering, Technology Innovation Center of Industrial Hemp for State Market Regulation, Qiqihar University, Wenhua Street 42, Qiqihar, Heilongjiang 161006, China
[3]Analysis and Testing Center, Qiqihar University, Wenhua Street 42, Qiqihar, Heilongjiang 161006, China
[4]Lead contact
*Correspondence: 02900@qqhru.edu.cn
https://doi.org/10.1016/j.isci.2024.108993

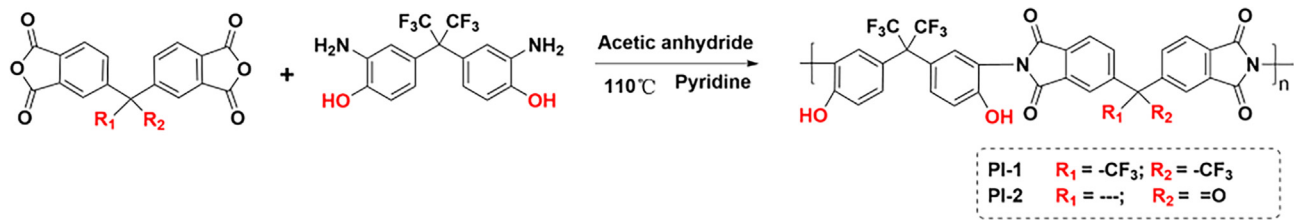

Scheme 1. Synthesis route of the polyimide precursors (PI-1 and PI-2).

As a branch of POPs materials, hypercrosslinked polymers (HCPs) exhibit their unique advantages, such as the simple preparation process and mild reaction conditions without any expensive catalyst. In addition, HCPs are predominantly porous and possess high surface specific surface areas, which also play a particularly important role in adsorption process.[31–35]

Polyimide is a kind of commercial material which can be directly synthesized by condensation of anhydrides and amines. Therefore, it contains abundant of electron-rich groups such as carbonyl groups, imides and benzene rings on the backbone and shows a promising prospect as precursor for iodine capture materials. Additionally, Ghosh et al. synthesized two hydroxy-functionalized (-OH) hypercrosslinked polymers (HCPs) and demonstrated that the hydroxyl groups in the polymers can form H-bonding with iodine and triiodide ions which further enhanced the iodine removal efficiency from water.[36] Neeladri Das et al. reported a facile triptycene based hydroxyl Azo-nanoporous polymer and the presence of phenolic-OH in the polymer enable it effective for iodine capture (1.88 g g^{-1}).[37] From these perspectives, two polyimide-based HCPs are developed by classical Friedel-Crafts alkylation reaction to introduce polar phenolic hydroxyl groups into the porous polymer networks, further increase the affinity between the HCPs and iodine molecules to enhance the iodine capture performance of the absorbents.

As expected, both polymers exhibit a remarkable capture capacity for volatile iodine as well as iodide ions from aqueous solution. In addition, the resulting polymers represent a good thermal and chemical stability, including recycling ability which endow them with a great potential for application in actual environmental treatment. To the best of our knowledge, PIHCP-1 shows the best iodine capture performance among the published HCP-based sorbents.

RESULTS AND DISCUSSION

Structure analysis

Two facile hydroxyl-functionalized HCPs were prepared as described in Schemes 1 and 2 and Fourier Transform infrared spectroscopy (FTIR) spectra was used to confirm the binding characteristic of the obtained polymers. Appearance of C-H stretching vibration of methylene groups at 2930 cm^{-1} in PIHCP-1 and PIHCP-2 proves the successful crosslinking of the polyimide precursors by Friedel-Crafts alkylation reaction.[38] As is well known, the band at 724 cm^{-1} is due to C-H out-of-plane bending vibration on benzene rings, hence, the significantly decrease of this vibration after the Friedel-Crafts alkylation reaction demonstrates successful crosslinking of the polyimides.[39,40] The C-N-C stretching of the imide group observed at approximately 1380 cm^{-1} and the asymmetrical and symmetrical stretching of C=O at 1781 cm^{-1} and 1733 cm^{-1} arises from the polyimide skeleton.[41] The observations above indicate the successful preparation of the target polymers.

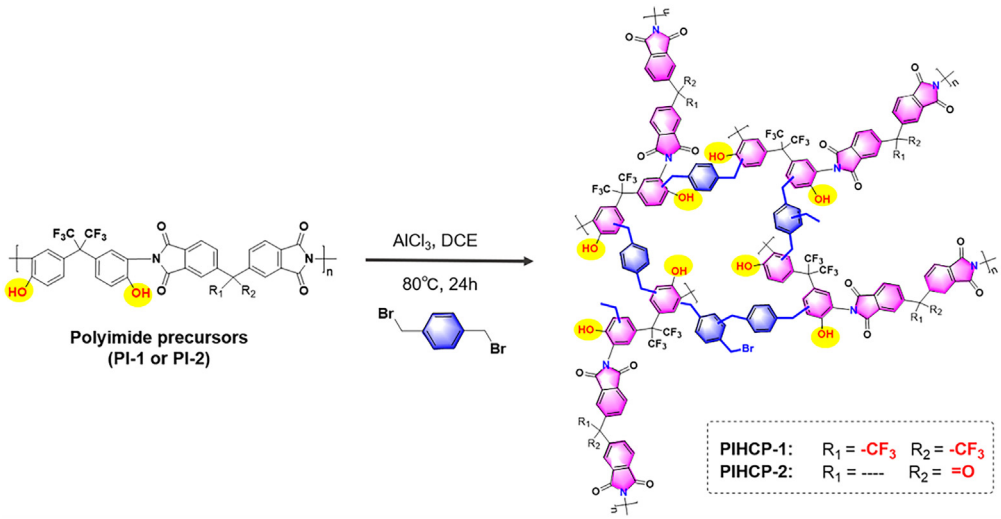

Scheme 2. Synthetic route for PIHCP-1 and PIHCP-2.

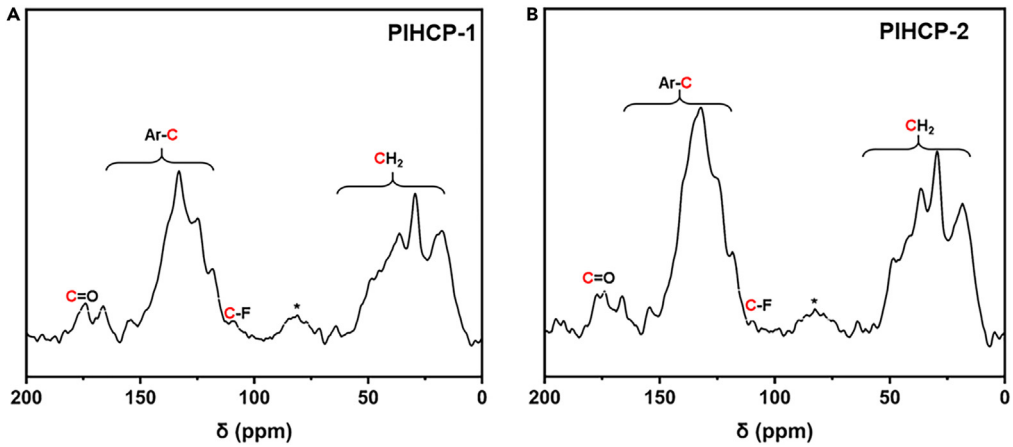

Figure 1. Solid-state ^{13}C NMR spectra of the adsorbents

(A) PIHCP-1.

(B) PIHCP-2.

To further identify the chemical structure of PIHCPs, solid-state ^{13}C cross-polarization magic-angle spinning NMR (CP-MAS) were taken (Figure 1). As expected, the characteristic chemical shift of carbons on benzene rings in the polymer is observed between 118 and 154 ppm. Meanwhile, the signal near 170 ppm can be attributed to carbonyl groups on the polyimide backbone[39] and the chemical shift observe at 109.8 ppm are arise from the carbon on C-F units.[42,43] In addition, the wide peak at 19–64 ppm belongs to the carbon atom of methylene on the crosslinker which further verify the crosslinking between the polymer chain to form the totally insoluble HCPs solid. In order to better applied in practice, stability of the PIHCPs in acidic, alkaline and organic reagents have also been evaluated. As shown in Table S1, the PIHCPs are totally insoluble and no swelling in common organic solvents indicating its good chemical stability. Besides, FTIR analysis was utilized to further clarify their stability after various solvents treatment (Figure S2). Apparently, the chemical structure of PIHCP-1 and PIHCP-2 has no obvious variation after immersing in various organic solvents, HCl and NaOH aqueous solutions (1M) and also have no degradation in acidic and alkaline conditions, which further proves their perfect chemical stability.

Morphology and thermal stability

To investigate the porosity of PIHCPs, nitrogen adsorption isotherms were performed at 77 K. As it shown in Figures 2A and 2C, both of PIHCP-1 and PIHCP-2 occurs a strong nitrogen adsorption at low relative pressure (P/P_0<0.03) indicating the permanent of microporosities. In addition, when the P/P_0 range from 0.8 to 1.0, the N_2 nitrogen adsorption increased rapidly which can be ascribed to the exitance of mesopores and macropores.[44,45] On the basis of IUPAC classification, we conclude that no matter PIHCP-1 or PIHCP-2 displays a mixed type-I/IV gas sorption isotherm.[46]

The BET surface area and total pore volume (P/P_0 = 0.99) were calculated to be 367.23 $m^2\ g^{-1}$ and 0.62 $m^3\ g^{-1}$ for PIHCP-1 and 357.26 $m^2\ g^{-1}$ and 0.214 $m^3\ g^{-1}$ for PIHCP-2, respectively. The average adsorption pore widths for the PIHCP-1 and PIHCP-2 were determined to be 5.562 nm and 1.076 nm, respectively. Moreover, the pore size distribution calculated by nonlocal density functional theory (NLDFT) shows that the pores in PIHCP-1 and PIHCP-2 are mainly centered at approximately 1.62 nm and 1.08 nm, respectively (Figures 2B and 2D). Detail data for the nitrogen adsorption and desorption of PIHCPs are summarized in Table 1. Furthermore, scanning electron microscopy (SEM) images also show that the PIHCP-1 is mainly composed of large amounts of irregular particles and stuck together to form a porous morphology, the particle sizes were approximately measured to be ranged from 100 to 200 nm (Figure 3A). In the case of PIHCP-2, it has a porous morphology consisting of agglomerated irregular particles that form a similar porous network (Figure 3B). Therefore, this porous morphology will greatly increase the free volume inside the polymer and ensure sufficient contact between iodine molecules and the active sites, meanwhile improve the mass transfer rate of the solution within the adsorbents to effectively improve the iodine adsorption performance of the polymers.

Thermal stability of the obtained PIHCPs was confirmed by Thermogravimetric analysis (TGA) under N_2 atmosphere and observed that both PIHCP-1 and PIHCP-2 show a greatly improved thermal stability compared with the polyimide precursor, it began to collapse near 300°C and the weight losses of PIHCP-1 is less than 44% until 800°C, which is slightly higher than that of PIHCP-2 (50%) (Figure S3). This excellent thermal stability can be attributed to the crosslinking between the polyimide main chains to form a three-dimensional network and is very crucial for their further practical application.[47]

Volatile iodine capture and adsorbent recycling

PIHCPs have a great potential in iodine absorption due to their porous structure, high thermal stability. Importantly, they contain a large amount of NH, F, C=O etc including polar -OH groups in their skeletons which can act as electron donor to interact with iodine molecules.[48–50] Thus, volatile iodine capture performance of PIHCPs were checked at 75°C by gravimetric analysis and the results are described in Figure 4A.

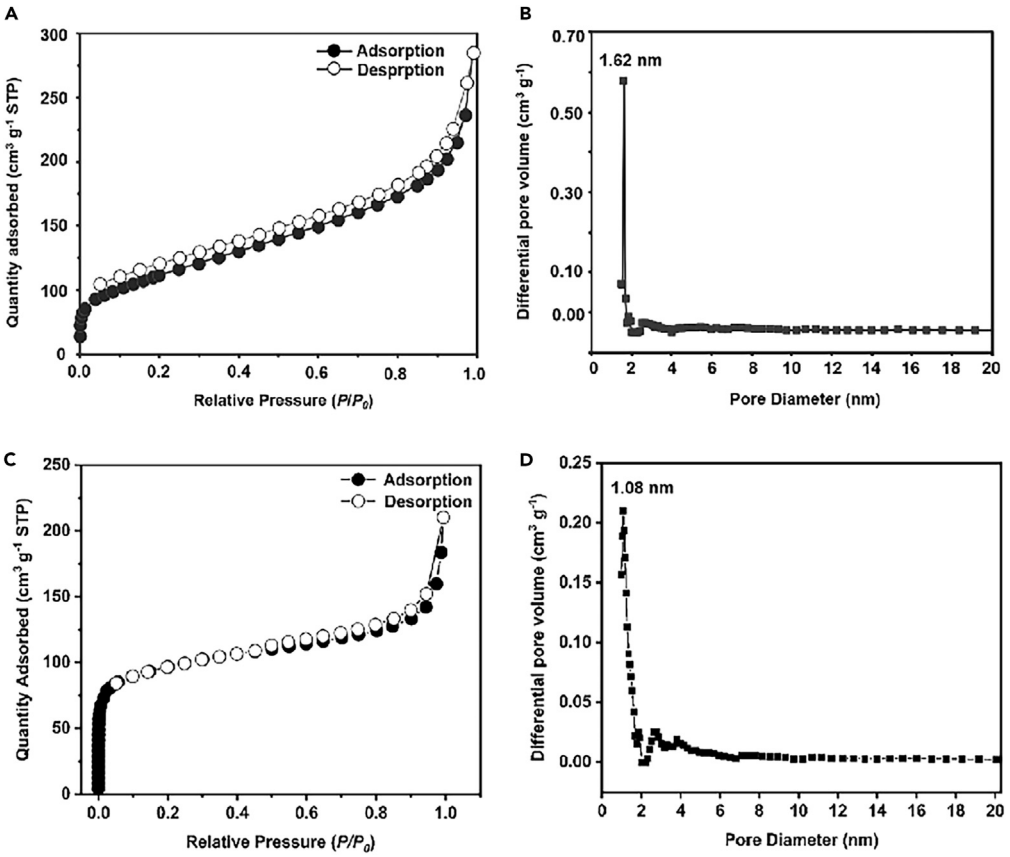

Figure 2. Porous characterization of PIHCPs

(A) and (C) Nitrogen adsorption-desorption isotherms of PIHCP-1 and PIHCP-2.

(B) and (D) Pore size distribution curve of PIHCP-1and PIHCP-2 (NLDFT).

Remarkably, both of PIHCP-1 and PIHCP-2 show a similar trend in the iodine capture process. First, the iodine uptake capacity of the polymers showed a dramatic increase within the first 3 h and nearly reach 78% of the equilibrium adsorption capacity for PIHCP-1 and approximately 82% for PIHCP-2. The maximum adsorption capacity is calculated to be 6.73 g g^{-1} and 6.11 g g^{-1} for PIHCP-1 and PIHCP-2, respectively.

For further discuss the iodine adsorption behavior of PIHCPs, iodine capture capacity of corresponding polyimide precursors (PI-1 and PI-2) was also evaluated as shown in Figure 4A. Obviously, the PI precursors have almost no ability for iodine capture (0.16 g g^{-1} and 0.12 g g^{-1}) which further proves that the porous structure caused by cross-linking between the polymer chains have a great contribution on their iodine adsorption performance. Results analysis show that the maximum equilibrium amount of iodine absorbed on PIHCP-1 is 6.73 g g^{-1}, which can be equated to a volume of 1.36 m^3 g^{-1} and is much higher than the pore volume (0.030 m^3 g^{-1}) calculated by NLDFT. This implies that the iodine capture capacity is not only related to their porous structure and specific surface area but also correlated to their actual content of binding sites, which can also greatly affect the adsorption performance. The higher content of electron-rich fluorine atoms in PIHCP-1 enriches the adsorption sites and leads to a stronger interaction between the polymer and iodine compared with PIHCP-2, hence, endows PIHCP-1 a higher iodine capture capacity.[51–54]

A comparison between the prepared PIHCPs and published POP absorbents used for iodine capture is summarized in Figure 4B. The result indicates that the iodine capture performance of PIHCPs is comparable to most of the published POP absorbents. This excellent iodine

Table 1. Textural properties of PIHCP-1 and PIHCP-2

Samples	[1]S_{BET} [m^2 g^{-1}]	[2]V_{total} [m^3 g^{-1}]	[3]V_{micro} [m^3 g^{-1}]	S_{micro} [m^2 g^{-1}]	D_{BJH} [nm]
PIHCP-1	367.2	0.620	0.030	64.1	5.562
PIHCP-2	357.3	0.214	0.104	250.6	1.076

[1]Surface area calculated from N_2 adsorption isotherms using the BET equation.

[2]Total pore volume at P/P_0 = 0.99.

[3]Micropore volume determined by DFT.

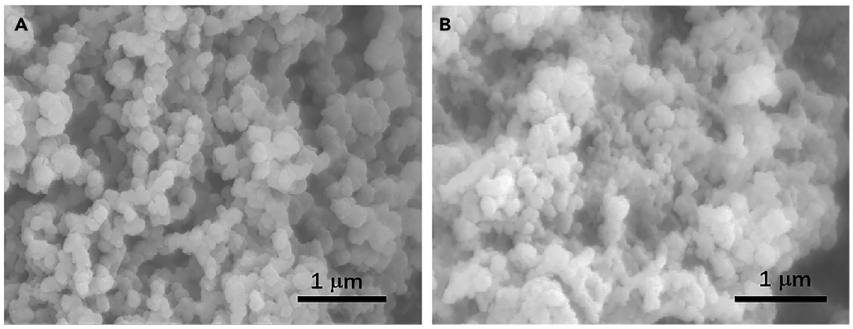

Figure 3. Morphology of PIHCPs

(A) and (B) SEM images of PIHCP-1 and PIHCP-2 (scale bar: 1 μm).

uptake capacity can be ascribed to the combined effects of the abundant electron donor sites on polyimide backbones and the porosity structure within the polymer.[46,47]

In view of the significant impact of iodine releasing ability and recyclability on the practical application of adsorbents, the releasing and recycling experiments were carried out as described in the experimental part. As shown in Figures 5A and S5, two maximum adsorption peaks are observed at 291 and 360 nm, which can be attributed to formation of polyiodide anion.[54] Moreover, the UV absorption intensity also graduate increased with the releasing time prolongs and it showed a linear release of iodine from PIHCP-1 and PIHCP-2 during the first 30 min implying the host-guest interaction releasing mechanism (Figure S5).[55,56] Finally, up to 97.8% of the captured iodine can be released from the absorbents for further cyclic utilization. As shown in Figure 5B, PIHCP-1 and PIHCP-2 can maintain 93.6% and 91.3% of their iodine capture capacity, respectively after four cycles indicating the perfect stability and recyclability for further utilization in practical nuclear waste disposal. Additionally, the chemical structure and porous morphology of recycled PIHCPs absorbents were further examined by FTIR spectra, nitrogen adsorption and SEM images. As described in Figures 5C and S6A, the recycled PIHCPs showed similar vibration peaks with the fresh samples, indicating its chemical stability during the application process. However, the specific BET surface area of the recovered PIHCPs after 4 cycles was found to be 53 $m^2\ g^{-1}$ for PIHCP-1 and 18 $m^2\ g^{-1}$ for PIHCP-2. The significant decrease in specific surface area was considered to be caused by the collapse of pores during repeated heating and cooling processes during the recycle experiments and residual iodine within the polymers.[57] Furthermore, SEM images of the spent PIHCP-1(Figure 5D) and PIHCP-2 (Figure S6B) also presented porous morphology after 4 cycles and the nitrogen adsorption shows similar textural properties (Figure S7). The above results confirm that the developed PIHCPs absorbent possess the excellent cyclability and structural stability.

Iodine adsorption

Depending on the perfect volatile iodine capture performance and insoluble property of PIHCPs in water and common solvents, the iodide ions removal efficiency of PIHCPs from solution were also evaluated for further treatment of radioactive iodine pollution in water environment. As presented in Figure 6A, both of PIHCP-1 and PIHCP-2 show a rapid iodine adsorption from cyclohexane solution within the incipient 3 h and reached adsorption equilibrium after 14 h. Meanwhile, color of the solution also shows a significant decolorization as the adsorption time

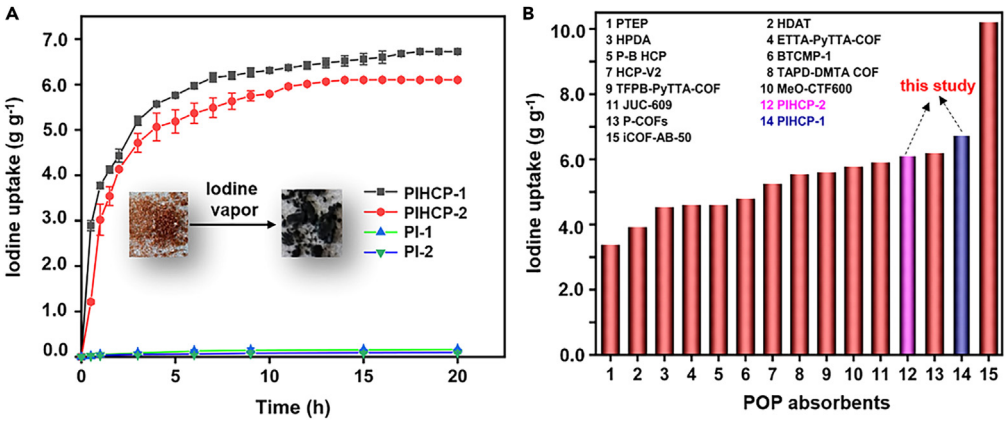

Figure 4. Volatile iodine capture performance of PIHCPs

(A) Volatile iodine capture curve for PIHCPs and corresponding polyimide precursors (inset: color changes of PIHCP-1 after exposed in iodine vapor for 14 h). Data are represented as means ± SDs, n = 3.

(B) Comparation of the iodine capture performance between PIHCPs with other POP absorbents.

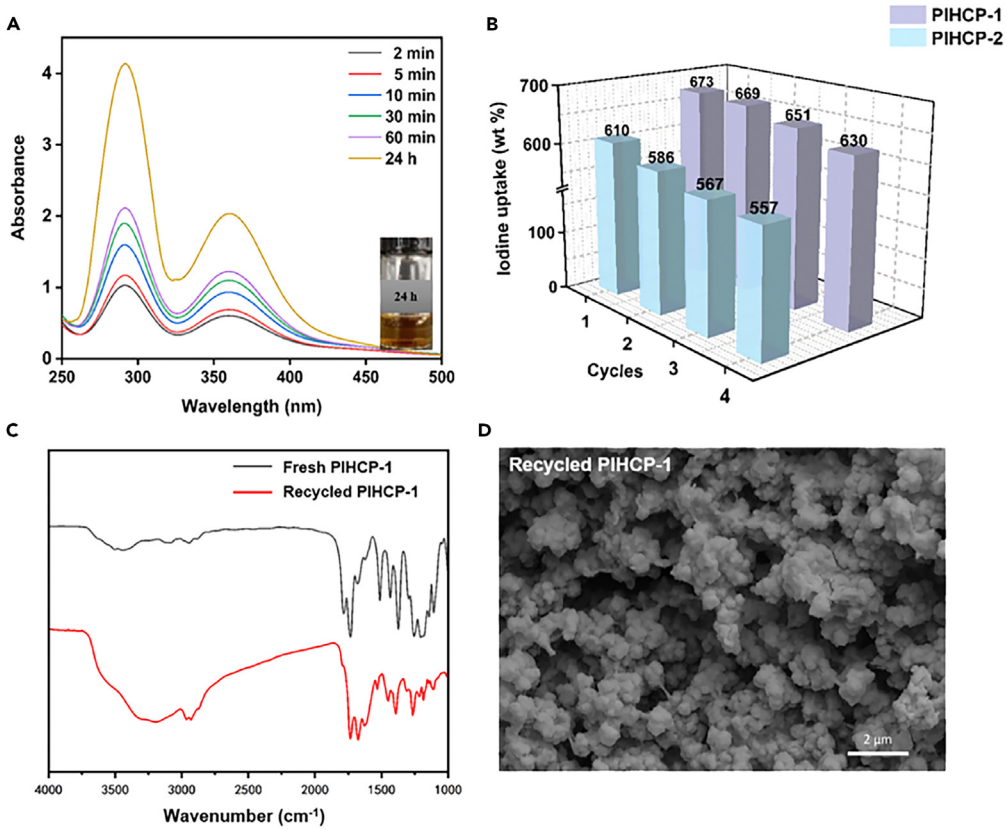

Figure 5. Iodine release, recyclability and structure characterization of spent adsorbents

(A) UV spectra of ethanol solution after PIHCP-1@I_2 immersed for different time (inset: color of the ethanol solution after 24 h).

(B) Recyclability of PIHCP-1 and PIHCP-2 for iodine capture. Data are represented as means ± SDs, n = 3.

(C) FTIR spectra of the fresh and recycled PIHCP-1.

(D) SEM image of recycled PIHCP-1 (scale bar: 2 μm).

prolongs (Figures 6A (inset) and S8). The maximum iodine removal efficiency was calculated by external standard method (Figure S9) to be 84.2% for PIHCP-1 and 77.9% for PIHCP-2, respectively and corresponding iodine adsorption amounts and UV/vis spectra are presented in Figures S10 and S11.

While in the case of aqueous solution, the PIHCPs represent a faster iodine adsorption and higher removal efficiency which can achieve 91% within 2 h and reach saturation after 4 h for PIHCP-1 (Figure 6B) also accompanied by an obviously color changes from yellow to colorless (Figures 6B (Inset) and S12). The maximum iodine removal efficiency for PIHCP-1 and PIHCP-2 in aqueous solution reached 99.7% and 92.5%, respectively. To deeply explore the reason of faster adsorption of iodine in aqueous media compared to organic media, the water contact angle of PIHCP-1 was evaluated and shown in Figure S3. Apparently, due to the presence of a large number of hydroxyl groups in the polymer structure, it exhibits an excellent hydrophilic property (water contact angle: 75.37°) which can promote the polymer better contact with the aqueous medium and further afford a better adsorption performance in aqueous solution.

It worth noting that regardless of volatile iodine capture or iodine ions adsorption in solution, PIHCP-1 exhibits a better adsorption performance compared with PIHCP-2, this phenomenon maybe caused by the higher content of fluorine atoms in the PIHCP-1 mainchain which will act as strong electron donating site to facilitate the interaction between the iodide ions and absorbent, in further endow PIHCP-1 a higher iodine accumulation capacity. A comparison of iodine uptake capacity and removal efficiency between PIHCPs and various porous materials have been summarized in Table S2. The PICHP-1 synthesized in this study showed an excellent volatile iodine uptake capacity which was 1.5–2 folders higher than that of the CMPs and COPs, and the iodine removal efficiency from aqueous and cyclohexane solutions was also higher than other porous organic polymers. Generally, the simple synthesis methods, readily available raw materials and excellent adsorption performance endow it great potentials in practical application.

Iodine adsorption mechanism

To specify the iodine capture process on the polymer absorbents and explain the adsorption mechanism, FTIR and X-ray Photoelectron Spectroscopy (XPS) spectra were examined and analyzed systematically. The FTIR spectra for PIHCPs and iodine-loaded PIHCPs

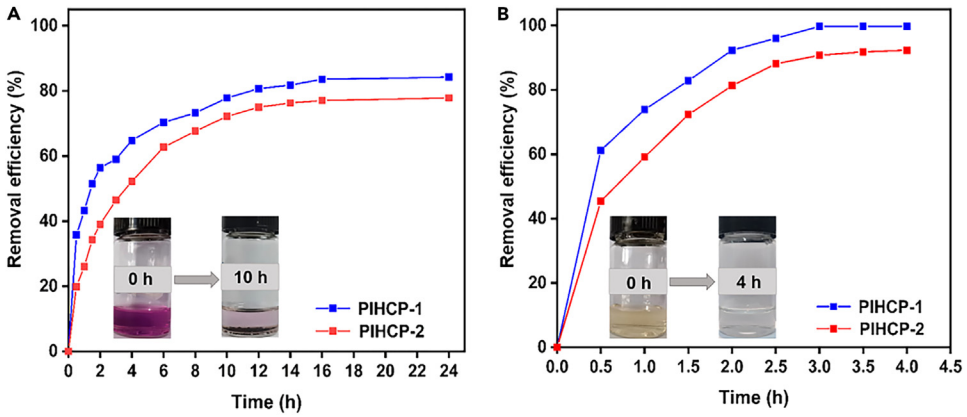

Figure 6. Iodine removal performance of PIHCPs in solution

(A) Iodine removal efficiency of PIHCPs from cyclohexane solution (40 mg/L) at different time intervals. (Inset: Color change of the cyclohexane solution after absorbed on PIHCP-1for 10 h). Data are represented as means ± SDs, n = 3.

(B) Iodine removal efficiency of PIHCPs from aqueous solution (40 mg/L) at different time intervals (Inset: Color change of the aqueous solution after absorbed on PIHCP-1 for 4h). Data are represented as means ± SDs, n = 3.

are shown in Figures 7 and S14. Taking PIHCP-1 as an example, the bands observed at 1729 cm^{-1}, 1382 cm^{-1}, 1254 cm^{-1} and 1666 cm^{-1} belong to stretching vibrations of C=O, C-N, C-F and skeleton vibrations of aromatic rings, respectively. The above-mentioned bands shift to 1717 cm^{-1}, 1374 cm^{-1}, 1249 cm^{-1} and 1652 cm^{-1} after absorption of iodine (Figure 7A) and PIHCP-2 also presents a similar band shift (Figure 7B). Similarly, the O-H vibration deriving from hydroxyl groups also shifted from 3445 cm^{-1} to 3400 cm^{-1} for PIHCP-1 and rom 3422 cm^{-1} to 3386 cm^{-1} for PIHCP-2, respectively after the iodine capture (Figure S14). This result proves the interaction between the absorbent and iodine molecules are mainly existed on the aromatic rings, carbonyl groups, imide sites, C-F units and hydroxyl groups in the polymer networks, which belong to electron-rich sites and can provide lone electron pairs that interact with iodine to form polyiodide anions. Afterward, this behavior leads to the above band-shift of the corresponding groups.[54,58]

X-Ray photoelectron spectroscopy (XPS) was employed to further analysis the surface elemental composition of PIHCP-1 and PIHCP-2. The corresponding diffraction peaks of C 1s, N 1s, I 3d and F 1s can be clearly observed in the survey scan XPS of PIHCPs (Figures S15A and S15B), indicating the successful adsorption of iodine within the polymer adsorbents. O 1s spectra of iodine loaded PIHCPs was further analyzed to confirm the binding sites within the adsorbents. As shown in Figures S15C and S15D, the peak at binding energy of 532.2 eV is attributed to the O-I and also suggest the formation of charge-transfer complex (O-I) when O-H functionalities interact with iodine.[59] Besides, high-resolution I 3d XPS of PIHCPs@I_2 were also examined to estimate the iodine adsorption process (Figures 7C and 7D). The characteristic I 3d absorption peaks indicates the existence of iodine within the polymers and the peaks at 618.7 and 630.3 eV, 620.6 eV and 631.7 eV arise from I_3^- and I_5^- anions also demonstrate that primary process of iodine absorption on PIHCPs is dominated by chemical adsorption.[55,58]

Raman spectra of PIHCPs and PIHCPs@I_2 are shown in Figure 8. Take PIHCP-1 as an example, the new absorptions at 105 and 141 cm^{-1} belong to the symmetrical and asymmetrical stretching vibration of I_3^- and the peak at 165 cm^{-1} is arise from stretching vibration of I_5^- which indicate that the absorbed I_2 in the HCP absorbent are presented in the form of I_3^- and I_5^-. In other words, the absorbed I_2 has been converted to polyiodide ions on account of the electron transfer from PIHCPs to iodine molecules.[10,58]

Combined with the results of FT-IR analysis, XPS, Raman, and iodine-released UV/vis spectrum, we can conclude that the iodine is absorbed on PIHCPs in the form of polyiodide. In other words, the hydroxyl groups and electron-rich heteroatoms in the polymer mainchain belong to Lewis bases which will easily interact with the Lewis acidic iodine molecular. This interaction is realized via charge transfer from electron-rich sites to antibonding molecular orbital (σ*) of I_2 and form the charge complex, in further absorb more iodine molecular to form polyiodide complex, PIHCP$^+I_3^-$ and PIHCP $^+I_5^-$, as shown in Scheme 3.

To get more insight into the iodine absorption mechanism, electrostatic potential (ESP) calculation was performed to analyze the surface charge environment of PIHCP-1 and PIHCP-2. As it shown in Figure 9, the maximum ESP values are observed at the H atom in the hydroxyl groups for PIHCP-1 and PIHCP-2. Besides, PIHCP-1 showed a maximum ESP value as 46.7 kcal mol^{-1} which 13.3 kcal mol^{-1} lower than that of PIHCP-2, and this lower ESP value contribute to weaken the n-π conjugation between the imide(carbonyl) groups and aromatic rings, in further enable the lone-pair electron on imide and carbonyl groups easier to bind with iodine molecules and resulted in a higher I_2 absorption capacity.[56,60] It is also in accordance with the experimental results.

In addition, the ESP value of oxygen atom on -OH groups present an extremely negative value in the whole unit indicate that the hydroxyl groups show a great contribution to form hydrogen bonds with the iodine/triiodide molecules during iodine adsorption process and further improve its iodine absorption capacity.[31]

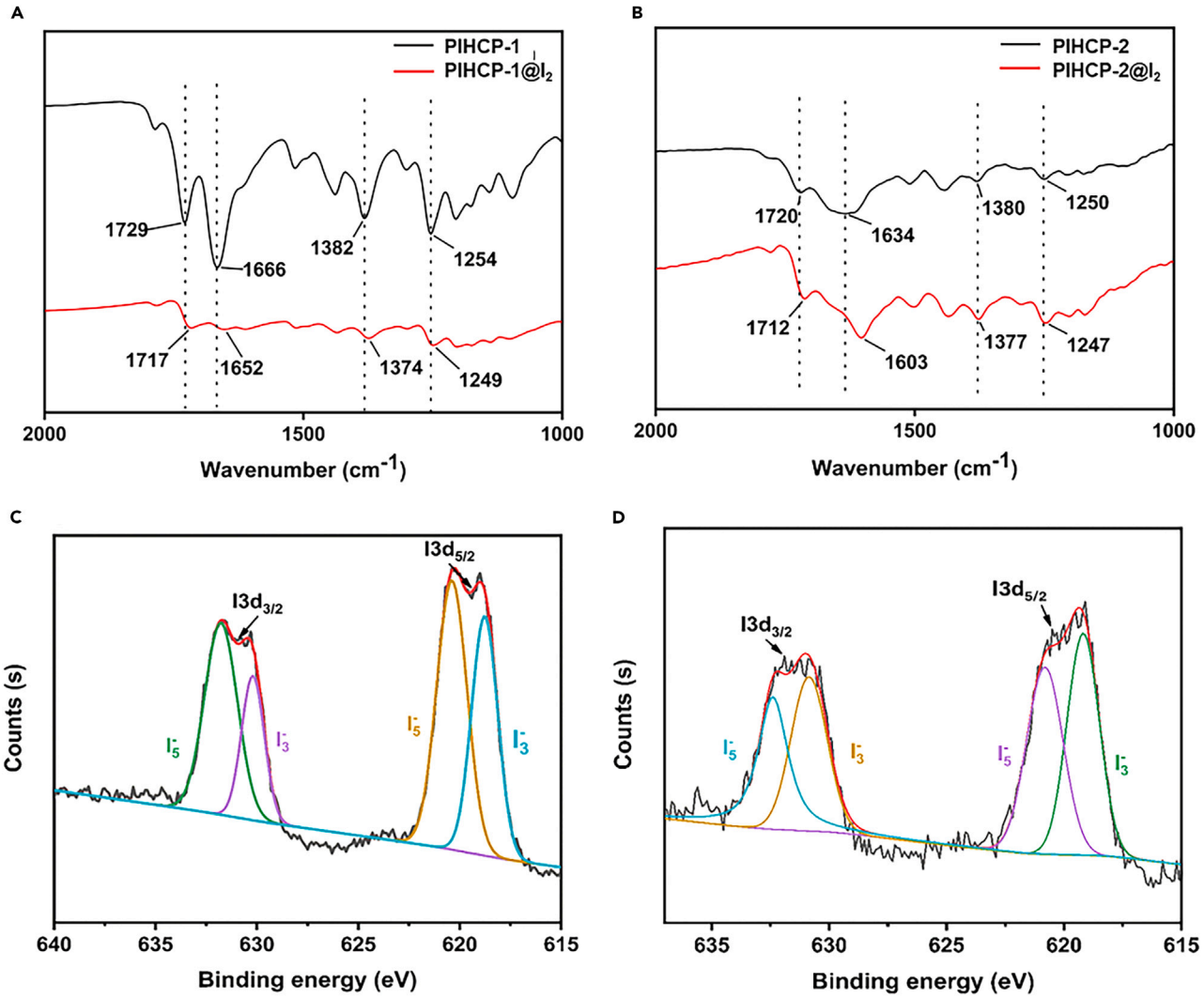

Figure 7. Characterization of the iodine-loaded PIHCPs

(A) and (B) FT-IR spectra of PIHCP-1@I_2 and PIHCP-2@I_2.

(C) and (D) I 3d peak splitting XPS spectra of PIHCP-1@I_2 and PIHCP-2@I_2.

Kinetic adsorption

Kinetic curves of iodine adsorption on PIHCPs are described to further investigate the mechanism and the models were calculated using Equations S1 and S2. As shown in Figure 10, the pseudo-second-order kinetic model for PIHCPs gives a higher correlation coefficient (R^2) than the pseudo-first-order model regardless of volatile iodine capture (Figures 10A and S16A) or removal of iodine from solution (Figures 10B, 10C, S16B, and S16C). In addition, taking volatile iodine capture as an example, the q_e values calculated by the pseudo-second-order kinetic model (6940 mg g^{-1}) are closer to the experimental result (6730 mg g^{-1}) than that by pseudo-first-order (6390 mg g^{-1}) (Tables S3 and S4), indicating the data above can be better fitted by the pseudo-second-order model and the iodine absorption on PIHCP-1 and PIHCP-2 are belong to the chemisorption-type processes.[60]

Adsorption isotherms

As is well known that Langmuir isotherm model presumes that the adsorbent surface is uniform and that the molecules are adsorbed onto the solid surface as a monolayer. In contrast, the Freundlich isotherm model assumes that the adsorption behavior occurs on the heterogeneous surface and involves multilayer adsorption.[61,62] Hence, two common isotherm models (Langmuir and Freundlich) were applied to analyze the adsorption type of iodine on the polymer absorbents and the experimental data were fitted by nonlinear models using Equations S3 and S4. Results suggest that no matter iodine adsorption from cyclohexane solution or aqueous solution by PIHCPs, the correlation coefficients of Freundlich model are higher than those of the Langmuir model (Figures 11 and S17; Table S5) which proves the iodine adsorption behavior

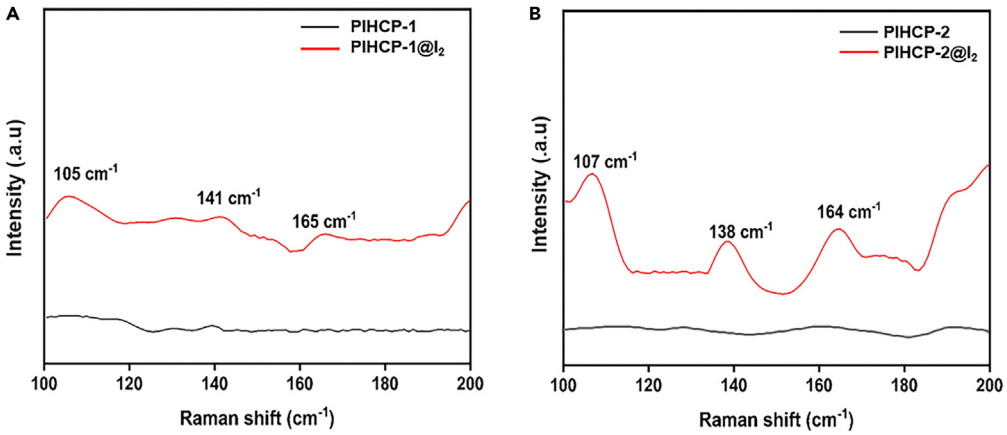

Figure 8. Raman spectra of iodine-loaded PIHCPs

(A) PIHCP-1@I_2.

(B) PIHCP-2@I_2.

is happen on the heterogeneous surfaces of PIHCPs as multilayer adsorption and the adsorption capacity of PIHCPs is very competitive in published HCP absorbents.[47] This excellent iodine adsorption performance of PIHCPs is considered to be arise from the combined effect of porous structure, high specific surface area and multiple active sites (hydroxyl groups, N and F atoms and aromatic rings) on the polyimide backbones.

Conclusions

In summary, two facile hydroxyl-functionalized HCPs with multi-active sites were synthesized and utilized in iodine adsorption. The resulting PIHCPs show a good thermal and chemical stability because of crosslinking between polymer chains to form a porous network. Relying on the functional hydroxyl groups and multiple electron donor sites in polyimide skeleton, the obtained absorbents show an excellent iodine capture

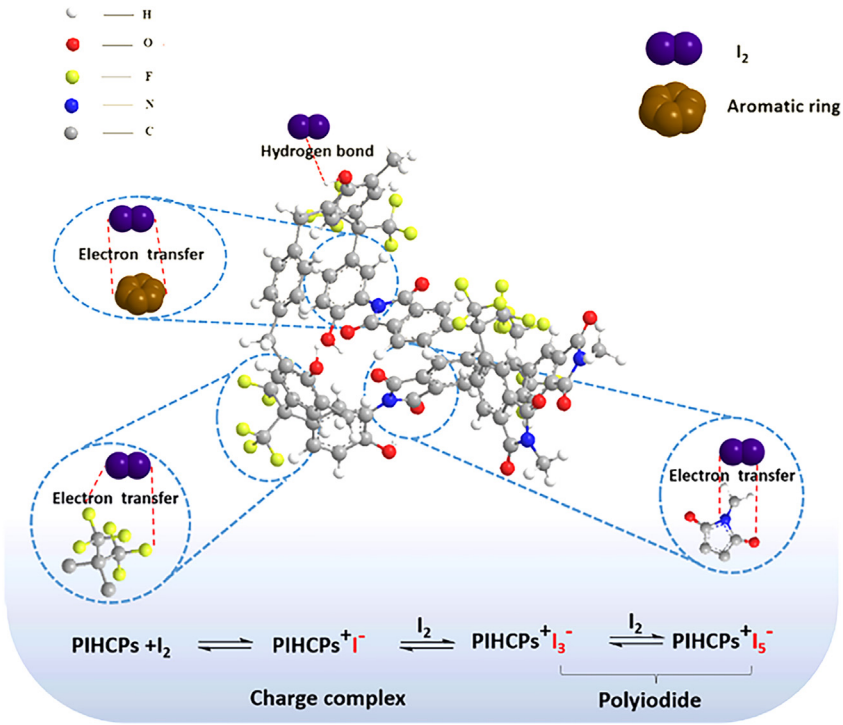

Scheme 3. Schematic illustration of the iodine uptake mechanism of PIHCPs.

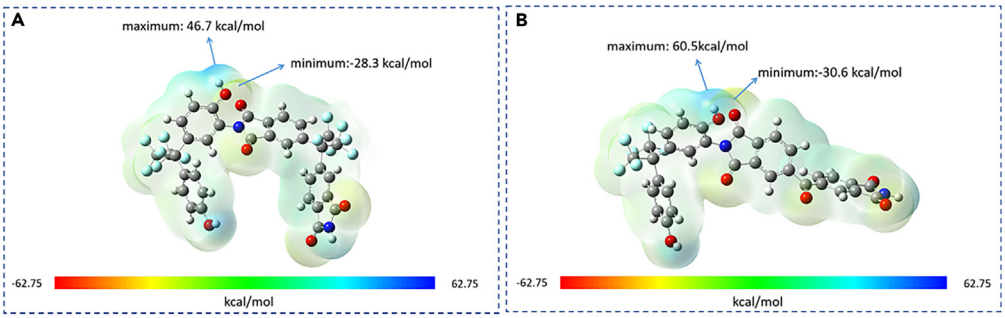

Figure 9. Electrostatic potential (ESP) mapping of PIHCPs

(A) and (B) Isodensity surface mappings of PIHCP-1 and PIHCP-2.

performance. The maximum volatile iodine capture capacity reached 6.73 g g^{-1} which is the highest one among published HCP absorbents and the iodine removal efficiency from aqueous solution reaches up to 99.7% within 3 h. ESP calculation indicates that the hydroxyl groups play an important role in enhancing the iodine adsorption ability which can form hydrogen bonds with the iodine/triiodide molecules during iodine adsorption process. Kinetics and adsorption isotherm results also clarify the chemisorption-type and multilayer processes on the heterogeneous surface. Hence, the present PIHCPs are especially attractive as iodine adsorbents for practical applications due to their high removal capacity, good recyclability and inexpensive synthesis method.

Limitations of the study

This study prepared PIHCP-1 and PIHCP-2, providing a new strategy for the development of iodine adsorbents suitable for both aqueous and organic solutions. However, this study also has limitations. The irradiation stability of the obtained adsorbents under irradiation has yet to be confirmed. In addition, there will be a need to develop materials that can be used for rapid iodine adsorption in multiple environments simultaneously in the future.

STAR★METHODS

Detailed methods are provided in the online version of this paper and include the following:

- KEY RESOURCES TABLE
- RESOURCE AVAILABILITY
  - Lead contact
  - Materials availability
  - Data and code availability
- METHOD DETAILS
  - Chemicals and materials

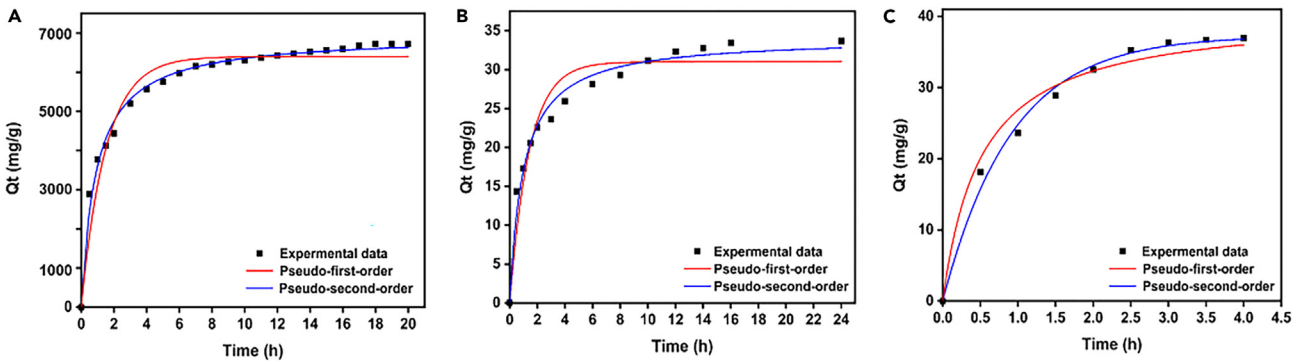

Figure 10. Analysis of the iodine adsorption kinetics behavior of PIHCP-1

(A) Volatile iodine capture. Data are represented as means ± SDs, n = 3.

(B) Iodine removal in cyclohexane solution. Data are represented as means ± SDs, n = 3.

(C) Iodine removal in aqueous solution. Data are represented as means ± SDs, n = 3.

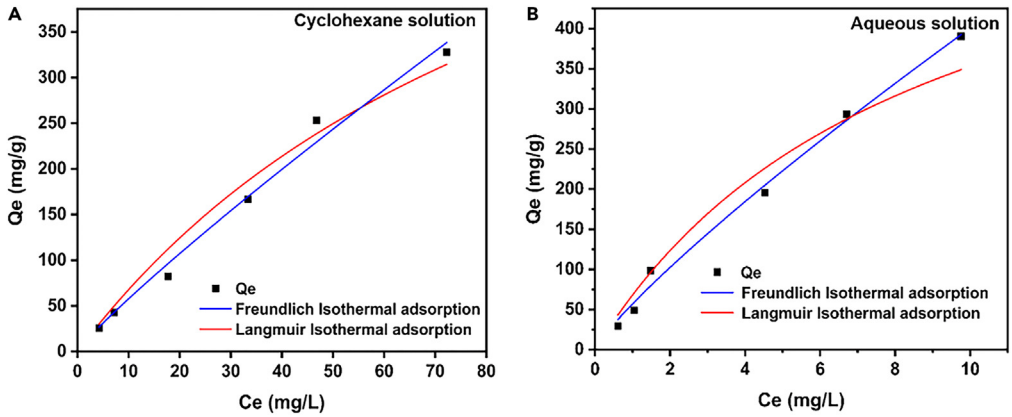

Figure 11. Iodine adsorption isotherms of PIHCP-2

(A) In cyclohexane solution. Data are represented as means ± SDs, n = 3.

(B) In aqueous solution. Data are represented as means ± SDs, n = 3.

- Characterization
- Synthesis of PIHCPs
- Iodine capture, release and recycle
- Iodine adsorption
- Kinetic adsorption
- Adsorption isotherms

- QUANTIFICATION AND STATISTICAL ANALYSIS

SUPPLEMENTAL INFORMATION

Supplemental information can be found online at https://doi.org/10.1016/j.isci.2024.108993.

ACKNOWLEDGMENTS

We acknowledge funding by National Natural Science Foundation of China (52173202); Fundamental Research Funds in Heilongjiang Provincial Universities (145109113); Technology Foundation for Selected Overseas Chinese, Ministry of Human Resources and Social Security of Heilongjiang Province ([2016] 75 (No.430237)); Heilongjiang Science Foundation Project (YQ2022E043).

AUTHOR CONTRIBUTIONS

Conceptualization, J.W. and Y.Z.; Methodology, T.W. and X.W.; Investigation; J.W., J.C., and M.F.; Writing–original draft, X.W. and T.W.; Writing–Review and editing, J.L. and Z.S.; Funding Acquisition, J.W. and Y.Z.; Supervision, L.X.

DECLARATION OF INTERESTS

The authors declare no competing interests.

Received: September 14, 2023
Revised: November 16, 2023
Accepted: January 18, 2024
Published: January 23, 2024

REFERENCES

1. Pan, T., Yang, K., Dong, X., Han, Y., and Han, Y. (2023). Adsorption-based capture of iodine and organic iodides, status and challenges. J. Mater. Chem. A *11*, 5460–5475. https://doi.org/10.1039/D2TA09448G.
2. Yu, Y.N., Yin, Z., Cao, L.H., and Ma, Y.M. (2022). Organic porous solid as promising iodine capture materials. J. Incl. Phenom. Macro. *102*, 395–427. https://doi.org/10.1007/s10847-022-01128-3.
3. Zhang, X., Maddock, J., Nenoff, T.M., Denecke, M.A., Yang, S., and Schröder, M. (2022). Adsorption of iodine in metal-organic framework materials. Chem. Soc. Rev. *51*, 3243–3262. https://doi.org/10.1039/D0CS01192D.
4. Zhang, Z., Li, L., An, D., Li, H., and Zhang, X. (2020). Triazine-based covalent organic polycalix[4]arenes for highly efficient and reversible iodine capture in water. J. Mater. Sci. *55*, 1854–1864. https://doi.org/10.1007/s10853-019-04164-6.
5. Yuan, K., Jiang, L., Zhang, J., and Zhang, J. (2022). Exploration synthesis and study of indol and pyridine-based heterocycle porous organic polytriazine for highly efficient iodine capture. J. Porous Mater. *29*, 405–413. https://doi.org/10.1007/s10934-021-01187-w.
6. Wang, X., Xie, L., Lin, K., Ma, W., Zhao, T., Ji, X., Alyami, M., Khashab, N.M., Wang, H., and

Sessler, J.L. (2021). Calix [4] pyrrole-crosslinked porous polymeric networks for the removal of micropollutants from water. Angew. Chem. Int. Ed. *60*, 7188–7196. https://doi.org/10.1002/anie.202016364.

7. Xu, X.H., Li, Y.X., Zhou, L., Liu, N., and Wu, Z.Q. (2022). Precise fabrication of porous polymer frameworks using rigid polyisocyanides as building blocks, from structural regulation to efficient iodine capture. Chem. Sci. *13*, 1111–1118. https://doi.org/10.1039/D1SC05361B.
8. Tian, Z., Chee, T.S., Zhu, L., Duan, T., Zhang, X., Lei, L., and Xiao, C. (2021). Comprehensive comparison of bismuth and silver functionalized nickel foam composites in capturing radioactive gaseous iodine. J. Hazard Mater. *417*, 125978. https://doi.org/10.1016/j.jhazmat.2021.125978.
9. Riley, B.J., Chong, S., Marcial, J., Lahiri, N., Bera, M.K., Lee, S., Wu, T., Kruska, K., and Matyáš, J. (2022). Silver-loaded xerogel nanostructures for iodine capture, a comparison of thiolated versus unthiolated Sorbents. ACS Appl. Mater. *5*, 9478–9494. https://doi.org/10.1021/acsanm.2c01741.
10. Shen, Z., Wiechert, A.I., Choi, S., Tavlarides, L.L., Tsouris, C., and Yiacoumi, S. (2022). Silver sulfide and silver sulfate as aging byproducts and adsorbents for gaseous iodine capture in spent nuclear fuel reprocessing. Ind. Eng. Chem. Res. *61*, 14393–14401. https://doi.org/10.1021/acs.iecr.2c02024.
11. Hu, H., Chen, F., Zhang, Z., Liu, D., Liang, Y., and Chen, Z. (2022). Heterometallic Metal-Organic Framework Based on $[Cu_4I_4]$ and $[Hf_6O_8]$ Clusters for Adsorption of Iodine. Front. Chem. *10*, 864131. https://doi.org/10.3389/fchem.2022.864131.
12. Wang, S.T., Liu, Y.J., Zhang, C.Y., Yang, F., Fang, W.H., and Zhang, J. (2023). Cluster-based crystalline materials for iodine capture. Chem. Eur J. *29*, e202202638. https://doi.org/10.1002/chem.202202638.
13. Zhang, Z.H., Ge, J.L., Li, Y., Li, Q., Ma, P.P., Tang, X.Y., Zhang, W.H., and Young, D.J. (2023). Two-dimensional Cd_3-based metal–organic frameworks with halogen bonding sites for the uptake of I_2. CrystEngComm *25*, 1775–1781. https://doi.org/10.1039/D2CE01582J.
14. Chaoui, N., Trunk, M., Dawson, R., Schmidt, J., and Thomas, A. (2017). Trends and challenges for microporous polymers. Chem. Soc. Rev. *46*, 3302–3321. https://doi.org/10.1039/c7cs00071e.
15. Wu, J., Xu, F., Li, S., Ma, P., Zhang, X., Liu, Q., Fu, R., and Wu, D. (2019). Porous polymers as multifunctional material platforms toward task-specific applications. Adv. Mater. *31*, e1802922. https://doi.org/10.1002/adma.201802922.
16. Lee, J.S.M., and Cooper, A.I. (2020). Advances in conjugated microporous polymers. Chem. Rev. *120*, 2171–2214. https://doi.org/10.1021/acs.chemrev.9b00399.
17. Giri, A., Khakre, Y., Shreeraj, G., Dutta, T.K., Kundu, S., and Patra, A. (2022). The order-disorder conundrum, a trade-off between crystalline and amorphous porous organic polymers for task-specific applications. J. Mater. Chem. A *10*, 17077–17121. https://doi.org/10.1039/d2ta01546c.
18. Das, N., Paul, R., Dao, D.Q., Chatterjee, R., Borah, K., Chandra Shit, S., Bhaumik, A., and Mondal, J. (2022). Nanospace engineering of triazine−thiophene-intertwined porous-organic-polymers via molecular expansion in tweaking CO_2 capture. ACS Appl. Nano Mater. *5*, 5302–5315. https://doi.org/10.1021/acsanm.2c00311.
19. Das, R., Paul, R., Parui, A., Shrotri, A., Atzori, C., Lomachenko, K.A., Singh, A.K., Mondal, J., and Peter, S.C. (2023). Engineering the charge density on an $In_{2.77}S_4$/porous organic polymer hybrid photocatalyst for CO_2-to-ethylene conversion reaction. J. Am. Chem. Soc. *145*, 422–435. https://doi.org/10.1021/jacs.2c10351.
20. Boro, B., Kalita, P., Vijayaprabhakaran, A., Dao, D.Q., Nandy, S., Chae, K.H., Nailwal, Y., Kathiresan, M., and Mondal, J. (2023). Discrete Cu-metalloporous polycarbazole as a nanoelectromediator for effective electrocarboxylation of benzyl bromide with CO_2. ACS Appl. Nano Mater. *6*, 11788–11801. https://doi.org/10.1021/acsanm.3c01721.
21. Xiong, S., Tang, X., Pan, C., Li, L., Tang, J., and Yu, G. (2019). Carbazole-bearing porous organic polymers with a mulberry-like morphology for efficient iodine capture. ACS Appl. Mater. Interfaces *11*, 27335–27342. https://doi.org/10.1021/acsami.9b07679.
22. Guo, X., Tian, Y., Zhang, M., Li, Y., Wen, R., Li, X., Li, X., Xue, Y., Ma, L., Xia, C., and Li, S. (2018). Mechanistic insight into hydrogen-bond-controlled crystallinity and adsorption property of covalent organic frameworks from flexible building blocks. Chem. Mater. *30*, 2299–2308. https://doi.org/10.1021/acs.chemmater.7b05121.
23. Chang, J., Li, H., Zhao, J., Guan, X., Li, C., Yu, G., Valtchev, V., Yan, Y., Qiu, S., and Fang, Q. (2021). Tetrathiafulvalene-based covalent organic frameworks for ultrahigh iodine capture. Chem. Sci. *12*, 8452–8457. https://doi.org/10.1039/d1sc01742j.
24. Wang, P., Xu, Q., Li, Z., Jiang, W., Jiang, Q., and Jiang, D. (2018). Exceptional iodine capture in 2D covalent organic frameworks. Adv. Mater. *30*, e1801991. https://doi.org/10.1002/adma.201801991.
25. Yan, J., Tong, S., Sun, H., and Guo, S. (2023). Nanoporous semi-cycloaliphatic polyaminal networks for capture of SO_2, NH_3, and I_2. J. Mater. Chem. A *11*, 6329–6335. https://doi.org/10.1039/D2TA10031B.
26. Wang, H., Qiu, N., Kong, X., Hu, Z., Zhong, F., Li, Y., and Tan, H. (2023). Novel carbazole-based porous organic polymer for efficient iodine capture and Rhodamine B adsorption. ACS Appl. Mater. Interfaces *15*, 14846–14853. https://doi.org/10.1021/acsami.3c00918.
27. Wang, K., Geng, T., and Zhu, F. (2023). The architectonics of bitetrazole-based porous organic polymers for capturing iodine and fluorescence sensing to iodine and 4-nitrophenol. Polym. Adv. Technol. *34*, 1529–1539. https://doi.org/10.1002/pat.5986.
28. Xie, Y., Pan, T., Lei, Q., Chen, C., Dong, X., Yuan, Y., Shen, J., Cai, Y., Zhou, C., Pinnau, I., and Han, Y. (2021). Ionic functionalization of multivariate covalent organic frameworks to achieve an exceptionally high iodine-capture capacity. Angew. Chem. Int. Ed. *60*, 22432–22440. https://doi.org/10.1002/ange.202108522.
29. Zhang, Y., Yi, D., Tu, P., Yang, S., Xie, Q., Gao, Z., Wu, S., and Yu, G. (2021). Boosting radioactive iodine capture of microporous polymers through strengthened host–guest interaction. Microporous Mesoporous Mater. *321*, 111148. https://doi.org/10.1016/j.micromeso.2021.111148.
30. Pourebrahimi, S., Pirooz, M., Visscher, A.D., and Peslherbe, G.H. (2022). Highly efficient and reversible iodine capture utilizing amorphous conjugated covalent triazine-based porous polymers, experimental and computational studies. J. Environ. Chem. Eng. *10*, 107850. https://doi.org/10.1016/j.jece.2022.107805.
31. Tan, L., and Tan, B. (2017). Hypercrosslinked porous polymer materials, design, synthesis, and applications. Chem. Soc. Rev. *46*, 3322–3356. https://doi.org/10.1039/c6cs00851h.
32. Huang, J., and Turner, S.R. (2018). Hypercrosslinked polymers, a review. Polym. Rev. *58*, 1–41. https://doi.org/10.1080/15583724.2017.1344703.
33. Li, H., Meng, B., Chai, S.H., Liu, H., and Dai, S. (2016). Hyper-crosslinked beta-cyclodextrin porous polymer, an adsorption-facilitated molecular catalyst support for transformation of water-soluble aromatic molecules. Chem. Sci. *7*, 905–909. https://doi.org/10.1039/c5sc04034e.
34. Shen, R., Yan, X., Guan, Y.J., Zhu, W., Li, T., Liu, X.G., Li, Y., and Gu, Z.G. (2018). One-pot synthesis of a highly porous anionic hypercrosslinked polymer for ultrafast adsorption of organic pollutants. Polym. Chem. *9*, 4724–4732. https://doi.org/10.1039/c8py01018h.
35. Giri, A., Biswas, S., Hussain, M.W., Dutta, T.K., and Patra, A. (2022). Nanostructured hypercrosslinked porous organic polymers, morphological evolution and rapid separation of polar organic micropollutants. ACS Appl. Mater. Interfaces *14*, 7369–7381. https://doi.org/10.1021/acsami.1c24393.
36. Samanta, P., Dutta, S., Let, S., Sen, A., Shirolkar, M.M., and Ghosh, S.K. (2022). Hydroxy-functionalized hypercrosslinked polymers (HCPs) as dual phase radioactive iodine scavengers, synergy of porosity and functionality. Chempluschem *87*, e202200212. https://doi.org/10.1002/cplu.202200212.
37. Ansari, M., Alam, A., Bera, R., Hassan, A., Goswami, S., and Das, N. (2020). Synthesis, characterization and adsorption studies of a novel triptycene based hydroxyl Azo-nanoporous polymer for environmental remediation. J. Environ. Chem. Eng. *8*, 103558. https://doi.org/10.1016/j.jece.2019.103558.
38. Li, X., Chen, G., and Jia, Q. (2019). One-pot synthesis of viologen-based hypercrosslinked polymers for efficient volatile iodine capture. Microporous Mesoporous Mater. *279*, 186–192. https://doi.org/10.1016/j.micromeso.2018.12.029.
39. Ansari, M., Hassan, A., Alam, A., and Das, N. (2021). A mesoporous polymer bearing 3D-Triptycene, -OH and azo-functionalities, reversible and efficient capture of carbon dioxide and iodine vapor. Microporous Mesoporous Mater. *323*, 111242. https://doi.org/10.1016/j.micromeso.2021.111242.
40. Tian, Y., Liu, L., Ma, F., Zhu, X., Dong, H., Zhang, C., and Zhao, F. (2021). Synthesis of phosphorylated hyper-cross-linked polymers and their efficient uranium adsorption in water. J. Hazard Mater. *419*, 126538–126549. https://doi.org/10.1016/j.jhazmat.2021.126538.
41. Wang, Y., Liu, L., Sang, K., Wang, Y., Zhang, C., Dong, H., and Bai, J. (2021). An efficient chiral porous catalyst support-Hypercrosslinked amino acid polymer. J. Catal. *404*, 411–419. https://doi.org/10.1016/j.jcat.2021.

42. Ong, Y.J., Pisharath, S., See, Y.F.A., Tay, C.Y., Hng, H.H., and Hng, H.H. (2022). Synthesis and characterization of a novel azido fuoroalkyl oligoether energetic plasticizer. J. Mater. Res. *37*, 1296–1308. https://doi.org/10.1557/s43578-022-00525-1.
43. Luo, Y., Yang, Z., Suo, X., Chen, H., Wang, T., Wang, Z., Liu, Y., Lyu, Y., Popovs, I., and Dai, S. (2021). Robust perfluorinated porous organic networks, Succinct synthetic strategy and application in chlorofluorocarbons adsorption. Nano Res. *14*, 3282–3287. https://doi.org/10.1007/s12274-021-3339-6.
44. Qian, X., Zhu, Z.Q., Sun, H.X., Ren, F., Mu, P., Liang, W., Chen, L., and Li, A. (2016). Capture and reversible storage of volatile iodine by novel conjugated microporous polymers containing thiophene units. Acs. Appl. Mater. Inter. *8*, 21063–21069. https://doi.org/10.1021/acsami.6b06569.
45. Wei, H., Wang, F., Qian, X., Li, S., Hu, Z., Sun, H., Zhu, Z., Liang, W., Ma, C., and Li, A. (2018). Superhydrophobic fluorine-rich conjugated microporous polymers monolithic nanofoam with excellent heat insulation property. Chem. Eng. J. *351*, 856–866. https://doi.org/10.1016/j.cej.2018.06.162.
46. Abdelmoaty, Y.H., Tessema, T.D., Choudhury, F.A., El-Kadri, O.M., and El-Kaderi, H.M. (2018). Nitrogen-rich porous polymers for carbon dioxide and iodine sequestration for environmental remediation. Acs. Appl. Mater. Inter. *10*, 16049–16058. https://doi.org/10.1021/acsami.8b03772.
47. Li, X., Chen, G., Ma, J., and Jia, Q. (2019). Task-specific synthesis for reversible capture of radioactive iodine. Sep. Purif. Technol. *210*, 995–1000. https://doi.org/10.1016/j.seppur.2019.115739.
48. Wang, Y., Tao, J., Xiong, S., Lu, P., Tang, J., He, J., Javaid, M.U., Pan, C., and Yu, G. (2020). Ferrocene-based porous organic polymers for high-affinity iodine capture. Chem. Eng. J. *380*, 122420. https://doi.org/10.1016/j.cej.2019.122420.
49. Dai, D., Yang, J., Zou, Y.C., Wu, J.R., Tan, L.L., Wang, Y., Li, B., Lu, T., Wang, B., and Yang, Y.W. (2021). Macrocyclic arenes-based conjugated macrocycle polymers for highly selective CO_2 capture and iodine adsorption. Angew. Chem. Int. Ed. *60*, 8967–8975. https://doi.org/10.1002/ange.202015162.
50. Zhu, Y., Ji, Y.J., Wang, D.G., Zhang, Y., Tang, H., Jia, X.R., Song, M., Yu, G., and Kuang, G.C. (2017). Bodipy-based conjugated porous polymers for highly efficient volatile iodine capture. J. Mater. Chem. *5*, 6622–6629. https://doi.org/10.1039/C7TA00026J.
51. Xie, L., Zheng, Z., Lin, Q., Zhou, H., Ji, X., Sessler, J.L., and Wang, H. (2022). Calix [4] pyrrole-based crosslinked polymer networks for highly effective iodine adsorption from water. Angew. Chem. Int. Ed. *61*, e202113724. https://doi.org/10.1002/ange.202113724.
52. Xu, M., Wang, T., Zhou, L., and Hua, D. (2020). Fluorescent conjugated mesoporous polymers with N, N-diethylpropylamine for the efficient capture and real-time detection of volatile iodine. J. Mater. Chem. A *8*, 1966–1974. https://doi.org/10.1039/C9TA11446G.
53. Liao, Y., Weber, J., Mills, B.M., Ren, Z., and Faul, C.F.J. (2016). Highly efficient and reversible iodine capture in hexaphenylbenzene-based conjugated microporous polymers. Macromolecules *49*, 6322–6333. https://doi.org/10.1021/acs.macromol.6b00901.
54. Li, X., Peng, Y., and Jia, Q. (2020). Construction of hypercrosslinked polymers with dual nitrogen-enriched building blocks for efficient iodine capture. Sep. Purif. Technol. *236*, 116260. https://doi.org/10.1016/j.seppur.2019.116260.
55. Xiong, S., Tao, J., Wang, Y., Tang, J., Liu, C., Liu, Q., Wang, Y., Yu, G., and Pan, C. (2018). Uniform poly (phosphazene-triazine) porous microspheres for highly efficient iodine removal. Chem. Commun. *54*, 8450–8453. https://doi.org/10.1039/C8CC04242J.
56. Zhang, J., Zhang, K., Liang, X., Yu, W., Ge, X., Shehzad, M.A., Ge, Z., Yang, Z., Wu, L., and Xu, T. (2021). Self-aggregating cationic-chains enable alkaline stable ion-conducting channels for anion exchange membrane fuel cells. J. Mater. Chem. A *9*, 327–337. https://doi.org/10.1039/D0TA11011F.
57. Shreeraj, G., Sah, A., Sarkar, S., Giri, A., Sahoo, A., and Patra, A. (2023). Structural modulation of nitrogen-rich covalent organic frameworks for iodine capture. Langmuir *39*, 16069–16078. https://doi.org/10.1021/acs.langmuir.3c02215.
58. Li, X., Chen, G., and Jia, Q. (2018). Highly efficient iodine capture by task-specific polyethylenimine impregnated hypercrosslinked polymers. J. Taiwan Inst. Chem. Eng. *93*, 660–666. https://doi.org/10.1016/j.jtice.2018.09.023.
59. Shi, Z., Huang, X., Zhao, Y., Li, J., Tian, Y.Q., Zhang, P.P., Zhu, M., and Zhao, M. (2023). Construction of a novel ursolic acid-based supramolecular gel for efficient removal of iodine from solution. Environ. Res. *235*, 116617. https://doi.org/10.1016/j.envres.2023.116617.
60. Geng, X., Ma, H., Lv, F., Yang, K., Ma, J., Jiang, Y., Liu, Q., Chen, D., Jiang, Y., and Zhu, N. (2022). Ultrastable organic cathode derived by pigment/rGO for aqueous zinc-ion batteries. Chem. Eng. J. *446*, 137289. https://doi.org/10.1016/j.cej.2022.137289.
61. Li, J., Xu, L., Sun, P., Zhai, P., Chen, X., Zhang, H., Zhang, Z., and Zhu, W. (2017). Novel application of red mud, facile hydrothermal-thermal conversion synthesis of hierarchical porous AlOOH and Al_2O_3 microspheres as adsorbents for dye removal. Chem. Eng. J. *321*, 622–634. https://doi.org/10.1016/j.cej.2017.03.135.
62. Foo, K.Y., and Hameed, B.H. (2010). Insights into the modeling of adsorption isotherm systems. Chem. Eng. J. *156*, 2–10. https://doi.org/10.1016/j.cej.2009.09.01316.
63. Zhu, G., Wang, F., Gong, X., Geng, P., Gao, Z., and Wang, Y. (2020). Preparation and alignment properties of photosensitive polyimide containing benzophenone in main chain. Liq. Cryst. *47*, 750–760. https://doi.org/10.1080/02678292.2019.1679902.
64. Huan, W., Huiping, H., and Qifan, P. (2021). Superior removal of iodine via cyclophosphazene-based conjugation-enriched cross-linking hybrid polymers. Colloid. Surface. *627*, 127185. https://doi.org/10.1016/j.colsurfa.2021.127185.

STAR★METHODS

KEY RESOURCES TABLE

REAGENT or RESOURCE	SOURCE	IDENTIFIER
Chemicals, peptides and recombinant proteins		
4-4′-(Hexafluoroisopropylidene)diphthalic anhydride	Aladdin	Cat#1107-00-2
1,2-dichloroethane	Aladdin	Cat#107-06-2
α,α′-dibromo-*p*-xylene	Aladdin	Cat#623-24-5
2,2′-Bis(3-amino-4-hydroxyphenyl)-hexafluoropropane	Innochem	Cat#83558-87-6
N-methyl-2-pyrrolidone	Innochem	Cat#2687-44-7
Pyridine	Acmec	Cat#110-86-1
Acetic anhydride	Kermel	Cat#108-24-7
Aluminum chloride	Macklin	Cat#7446-70-0
Hydrochloric acid	Quanrui	Cat#7647-01-0
Other		
Fourier transformed infrared	JASCO	FT/IR-4200
Thermal gravity analysis	Waters	Q5000IRS
1H Nuclear Magnetic Resonance spectroscopy	Bruker	AVANCE-600
X-ray photoelectron spectroscopy	KRATOS	XSAM800
Automated Surface Area and Pore Size Analyzer	Quantachrome	NOVA4200e
Scanning electron microscopy	HITACHI	S-4300
UV–vis absorption spectra	PerkinElmer	Lambda 900

RESOURCE AVAILABILITY

Lead contact

Further information and requests for resources should be directed to and will be fulfilled by the lead contact, Jianjun Wang (02900@qqhru.edu.cn).

Materials availability

This study did not generate new unique reagents.

Data and code availability

All data reported in this paper will be shared by the lead contact upon request.

This paper does not report original code.

Any additional information required to reanalyze the data reported in this paper is available from the lead contact upon request.

METHOD DETAILS

Chemicals and materials

4-4′-(Hexafluoroisopropylidene)diphthalic anhydride (6FDA), 1,2-dichloroethane (AR, 99%) and α,α′-dibromo-p-xylene were provided by Aladdin (Shanghai, China). 2,2′-Bis(3-amino-4-hydroxyphenyl)-hexafluoropropane (AHHFP) and N-methyl-2-pyrrolidone (NMP, >99.5%) were obtained from Innochem (Beijing, China). Pyridine (Py) was provided by Acmec (Shanghai, China). Acetic anhydride (Ac_2O) was used as received from Kermel (Tianjin, China). Aluminum chloride was provided by Macklin (Shanghai, China), and hydrochloric acid (AR) was obtained from Quanrui (Liaoning, China). All solvents and chemicals were used as received without further purification.

Characterization

Fourier transformed infrared (FTIR) spectra were carried out on a JASCO FT/IR-4200 spectrometer. Thermal gravity analysis (TG) measurements were determined with a Q5000IRS analyzer. The analysis was performed with approximately 10 mg dried samples in a dynamic nitrogen atmosphere at a heating rate of 10°C min^{-1} from room temperature to 800°C. 1H NMR (600 MHz) spectra were recorded on a Bruker AVANCE-600

spectrometer. The nature of iodine element loaded on HCPs was recorded on an X-ray photoelectron spectrometer (XPS, XSAM800 spectrometer). Nitrogen adsorption-desorption isotherms were determined at 77 K with a Quantachrome Nova 4200e analyzer. Brunner–Emmett–Teller (BET) equation was used to calculate the cumulative apparent surfaces areas. Pore size distributions were derived from nitrogen adsorption-desorption isotherms using nonlocal density functional theory (NLDFT). Scanning electron microscopy (SEM) images were recorded on a HITACHI S-4300 electron microscope. UV–vis absorption spectra were collected on Lambda 900 spectrophotometer.

Synthesis of PIHCPs

The polyimide precursors (PI-1, PI-2) containing phenolic hydroxyl groups used for this study were prepared by polycondensation of AHHFP and 6FDA as it shown in Scheme 1 [63] (Mw = 2.1×10^4, Mw/Mn = 1.6 for PI-1 and Mw = 1.8 ×10^4, Mw/Mn = 2.0 for PI-2). Then, two facile hydroxyl-functionalized HCPs (PIHCP-1 and PIHCP-2) were synthesized via a classical Friedel-Crafts alkylation reaction using α,α′-dibromo-*p*-xylene as crosslinker and $AlCl_3$ as catalyst (Scheme 2). Taking PIHCP-1 as an example, a typical process was conducted as follow: PI-1 (0.42 g, 0.50 mmol) and $AlCl_3$ (1.3 g, 8.0 mmol) were added to a three-necked bottle with N_2 atmosphere and α,α′-dibromo-*p*-xylene (0.32 mg, 1.20 mmol) dissolved in dry DCE (10 mL) was injected into the reaction system. After stirring at 80°C for 24 h, the polymerization was quenched with HCl-H_2O (V_{HCl}/V_{H2O} = 2:1) (20 mL) and precipitated in deionized water to separate the polymer. After filtration, the obtain polymer was purified by Soxhlet extraction with dichloromethane as eluents and dried at 90°C for 48 h to obtained PIHCP-1 a brown solid (yield: 84.0%). PIHCP-2 followed the same procedure described above to obtain it as a light brown solid (yield: 70.5%).

Iodine capture, release and recycle

The volatile iodine capture capacity of PIHCPs was evaluated using gravimetric analysis.[58] To simulate a real nuclear fuel postprocessing environment, the open glass bottle (50 mL) with polymer absorbent (PIHCP-1 or PIHCP-2) was placed in a sealed bottle (500 mL) involving a certain amount of solid iodine, and the capture experiment in this system was carried out at 75°C and ambient pressure. After adsorption for a period of time, the system was cooled to room temperature, and the iodine-loaded PIHCPs were weighed for further calculation according to Equation 1:

$$\text{Iodine uptake capacity (wt \%)} = \frac{W2 - W1}{W1} \quad \text{(Equation 1)}$$

where W_1 and W_2 represent the original weight of the absorbent and its weight after iodine capture, respectively.

For iodine release, the iodine-loaded PIHCPs used in capture measurement above was immersed in ethanol for different time intervals and the supernatant was monitored using UV-2600 to determine the release efficiency. Besides, one of the iodine-loaded absorbents was soaking in ethanol overnight, washed with ethanol for several time and dried in vacuo at 120°C for 24 h to further investigate the recycling performance.

Iodine adsorption

The PIHCPs powder (10 mg) was added into the cyclohexane or aqueous solution with a certain iodine concentration (40 mg/L) and the residual iodine amount at different time intervals were examined by UV-vis spectra to further calculate the removal efficiency.[64]

Kinetic adsorption

Pseudo-first-order and Pseudo-second-order were used to characterize the kinetic process of iodine adsorption on PIHCPs and calculated using Equations S1 and S2 as follows:

pseudo-first-order:

$$\ln(q_e - q_t) = \ln q_e - k_1 t \quad \text{(Equation S1)}$$

pseudo-second-order:

$$\frac{t}{q_t} = \frac{1}{kq_e^2} + \frac{t}{q_e} \quad \text{(Equation S2)}$$

where q_e (mg g^{-1}) represents the equilibrium adsorption capacity and q_t (mg g^{-1}) is the iodine capture capacity at time t (min). k_1 (min^{-1}) and k (g mg^{-1} min^{-1}) stand for the pseudo-first-order and pseudo-second-order rate constants, respectively.

Adsorption isotherms

Freundlich and Langmuir isotherm models were used to characterize the adsorption process. The experimental data were fitted by nonlinear Langmuir and Freundlich models using Equations S3 and S4:

Langmuir model:

$$q_e = \frac{abC_e}{1+bC_e} \quad \text{(Equation S3)}$$

Freundlich model:

$$q_e = k_F(C_e)^{1/n} \quad \text{(Equation S4)}$$

Where C_e is the concentration of I_2 at equilibrium, q_e represents the corresponding adsorption capacity, a is the maximum adsorption capacity (mg g^{-1}), b is a constant related to the affinity of the active binding sites (L·mg^{-1}), k_F is the binding constant, which depends on the relative adsorption capacity of the adsorbent (mg g^{-1}), and (1/n) is the adsorption intensity.

QUANTIFICATION AND STATISTICAL ANALYSIS

All experiments in the adsorption kinetics, isothermal and thermodynamic studies were repeated three times and averaged for model fitting. The coefficients of determination (R^2) were used to determine the fitting effect. All other experiments were repeated three times and data are represented as means ± SDs.